Supplementary Material

Low Temperature CO Catalytic Oxidation and Kinetic Performances of KOH-Hopcalite in the Presence of CO_2

Yafei Guo [a], Changhai Li [a], Shouxiang Lu [a] Chuanwen Zhao [b] **

[a] State Key Laboratory of Fire Science, University of Science and Technology of China, Hefei 230026, China

[b] Jiangsu Provincial Key Laboratory of Materials Cycling and Pollution Control, School of Energy and Mechanical Engineering, Nanjing Normal University, Nanjing 210042, China

*Corresponding author:

Shouxiang Lu, Tel.: +86 551 63603141, Fax: +86 551 63601669, E-mail: sxlu@ustc.edu.cn

Chuanwen Zhao, Tel.: +86 551 63603141, Fax: +86 551 63601669, E-mail: cwzhao@ustc.edu.cn

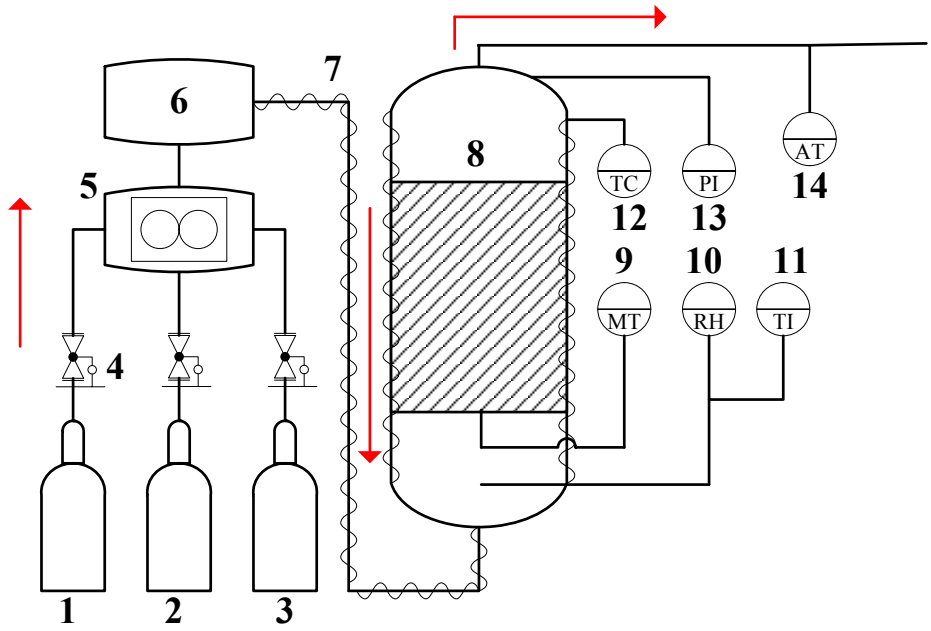

Fig. S0. Schematic of the experimental setup

(1) Compressed air; (2) CO; (3) CO_2; (4) pressure regulating valve; (5) mass flow controller; (6) mixture tank; (7) evaporator; (8) fixed-bed reactor; (9) mass transmitter; (10) relative humidity monitor; (11) temperature indicator; (12) temperature controller; (13) pressure indicator; (14) gas analyzer.

The experimental setup is shown in Fig. S0. The apparatus consists of three parts as a gas production system, a fixed-bed reactor and a measurement system. CO, CO_2 and compressed air were obtained from high purity cylinders with mass flow controllers to manipulate the flow rates. The gas mixtures then flowed into an electrical heater tank for uniform mixing before flowing through the fixed-bed reactor. In the reaction system, a fixed-bed reactor with an inner diameter of 0.02 m and a height of 0.2 m was included. For the measurement system, a thermocouple and a pressure gauge were equipped to monitor the temperature and pressure change in the reactor. The thermo-hydrometer was mainly for monitoring the moisture content and temperature of the mixing gases at the inlet of the reactor. A mass sensor was installed at the bottom of the reactor to monitor the mass change of samples, and a gas analyzer was equipped for on-line CO monitoring at the outlet of the reactor. In this way, the CO oxidation performances of the samples were evaluated.

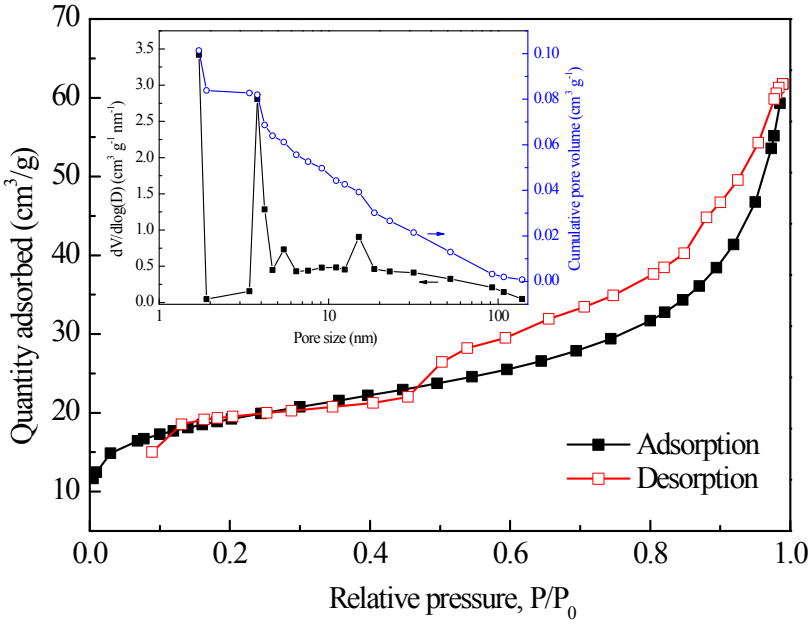

Fig. S1. N_2 adsorption-desorption isotherm and pore size distribution of KOH-Hopcalite

Fig. S1 presents the isotherm and pore diameter distribution of the catalyst. The isotherm of the prepared catalyst belongs to type IV, as an indicative of mesoporous material. Slight N_2 uptake under lower partial pressure is mainly depended on monolayer adsorption. The quantity of N_2 adsorbed significantly increases in high partial pressure area, due to the capillary condensation of the adsorbate. Besides, obvious H3 hysteresis loop could be observed when relative pressure is higher than 0.4. This implies that the pores in the catalyst are mainly cylindrical vents lying in narrow range of radius. The pore size distribution curve of the sample shows three peaks assigned in the pore size range of 0-2, 2-5, and 10-20 nm, indicating that the pores contained in the sample are mainly micropores and mesopores. Fig. S1 also shows the change of cumulative pore volume with pore size. With the decrease of pore size from 140 to 50 nm, the cumulative pore volume slightly increases to 0.0129 cm^3/g. A further decrease of pore size to 2 nm will lead to an increase of cumulative pore volume to 0.0826 cm^3/g. The mesopore volume is determined as 0.0697 cm^3/g, accounting for 84.12% of the total pore volume. This indicates that the majority of the pores are attributed as mesopores.

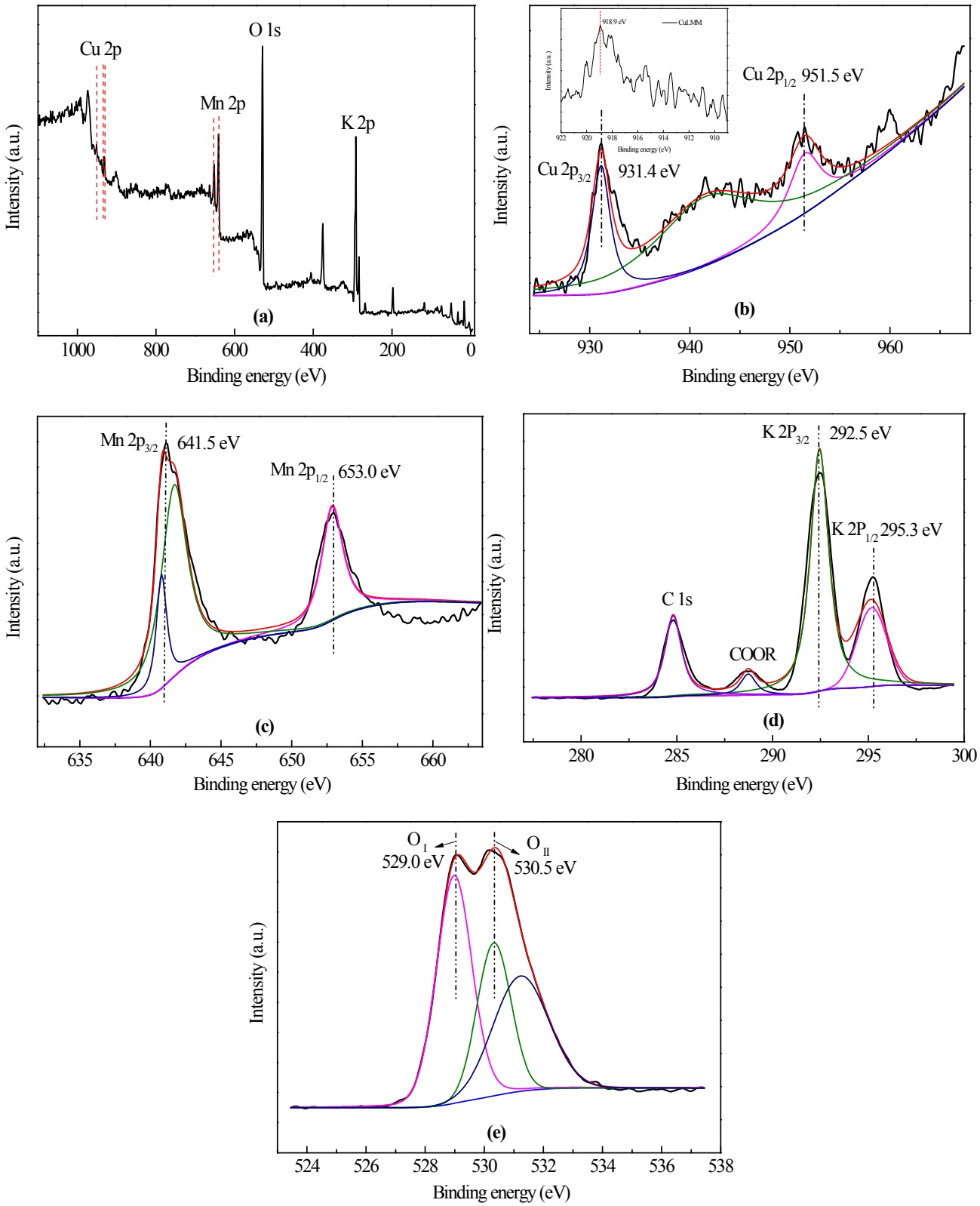

Fig. S2. XPS spectra of Cu_{2p}, Mn_{2p}, K_{2p} and O_{1s} regions of KOH-Hopcalite catalyst.

(a) survey spectra; (b) Cu_{2p} spectra; (c) Mn2p spectra; (d) K2p spectra; (e) O1s spectra

Fig. S2(a) displays the XPS survey spectrum of the catalyst. It can be observed that there are several characteristic peaks present in the survey spectrum, which are corresponding to different species as Cu 2p, Mn 2p, K 2p and O 1s. Fig. S2(b) shows the XPS spectrum of Cu 2p. The binding energy at 931.4 eV should be assigned as Cu $2p_{3/2}$. The satellite characteristic peak present at 951.5 eV is

attributed to Cu $2p_{1/2}$. These indicate that CuO is the primary oxidation state for Cu species. Fig. S2(c) presents the Mn 2p profile of the catalyst. The characteristic peaks at 641.5 and 653.0 eV are corresponding to Mn $2p_{3/2}$ and Mn $2p_{1/2}$, respectively. The binding energy for Mn^{3+} is reported in the range of 641.3-641.7 eV, while that for Mn^{4+} is 642.2-643.0 eV. This indicates that Mn_2O_3 is the major oxidation state for Mn species, and no evidence is provided for the presence of MnO_2. In order to determine the states of K species, the XPS spectrum of K 2p is provided in Fig. S2(d). The characteristic peaks at 292.5 and 295.3 eV are assigned as K $2p_{3/2}$ and K $2p_{1/2}$, respectively, as an indicative of the presence of K^+. The XPS spectrum of O 1s shows double-peak distributions. It is indicated that the binding energy for lattice oxygen ion O^{2-} (O_I) is 528.8-529.5 eV, and the binding energy for superoxide ion O^- (O_{II}) is 530.6-531.9 eV. The superoxide ion O^- could further form OH^-. The characteristic peak at 529.0 eV is attributed to the lattice oxygen ion O_I contained in the oxidation states of CuO and Mn_2O_3. The peak at 530.5 eV is detected as superoxide ion O_{II} in the form of OH^- presented in KOH. No characteristic peak of superoxide ion O^{2-} (III) (532.0-533.3 eV) could be observed in the spectrum of O 1s. It can be concluded that the main characteristic peaks of the sample are assigned as Cu 2p, Mn 2p, K 2p and O 1s.